

# OH-Formation Following Vibrationally Induced Reaction Dynamics of $\text{H}_2\text{COO}$

Kaisheng Song,<sup>1, a)</sup> Meenu Upadhyay,<sup>1</sup> and Markus Meuwly<sup>1, b)</sup>

*Department of Chemistry, University of Basel, Klingelbergstrasse 80,  
CH-4056 Basel, Switzerland*

(Dated: 16 February 2024)

The reaction dynamics of  $\text{H}_2\text{COO}$  to form linear  $\text{HCOOH}$  and dioxirane as first steps for OH-elimination is quantitatively investigated. Using a machine learned potential energy surface at the CASPT2/aug-cc-pVTZ level of theory vibrational excitation along the CH-normal mode  $\nu_{\text{CH}}$  with energies up to 40.0 kcal/mol ( $\sim 5\nu_{\text{CH}}$ ) leads almost exclusively to linear  $\text{HCOOH}$  which further decomposes into OH+HCO. Although the barrier to form dioxirane is only 21.4 kcal/mol the reaction probability to form dioxirane is two orders of magnitude lower if the CH-stretch mode is excited. Following the dioxirane-formation pathway is facile, however, if in addition the COO-bend vibration is excited with energies equivalent to  $\sim (2\nu_{\text{CH}} + 4\nu_{\text{COO}})$  or  $\sim (3\nu_{\text{CH}} + \nu_{\text{COO}})$ . For OH-formation in the atmosphere the pathway through linear  $\text{HCOOH}$  is probably most relevant because the alternative pathways (through dioxirane or formic acid) involve several intermediates that can de-excite through collisions, relax *via* Intramolecular vibrational energy redistribution (IVR), or pass through very loose and vulnerable transition states (formic acid). This work demonstrates how, by selectively exciting particular vibrational modes, it is possible to dial into desired reaction channels with a high degree of specificity for a process relevant to atmospheric chemistry.

---

<sup>a)</sup>School of Chemistry and Chemical Engineering, Chongqing University, Chongqing 401331, China

<sup>b)</sup>m.meuwly@unibas.ch

## I. INTRODUCTION

The photodissociation dynamics of small molecules is of fundamental interest in atmospheric chemistry. One of the chemically most relevant agents is the hydroxyl radical (OH)<sup>1</sup> which was also referred to as the “detergent of the troposphere”.<sup>2,3</sup> The radical triggers degradation of pollutants including volatile organic compounds (VOCs) and is an important chain initiator in most oxidation processes in the atmosphere. The amount of OH generated from alkene ozonolysis is an important determinant required for chemical models of the lower atmosphere. Field studies have suggested that ozonolysis of alkenes is responsible for the production of about one third of the atmospheric OH radicals during daytime, and is the predominant source of OH radicals at night.<sup>4,5</sup> Alkene ozonolysis proceeds through a 1,3-cycloaddition of ozone across the C=C bond to form a primary ozonide which then decomposes into carbonyl compounds and energized carbonyl oxides, known as Criegee Intermediates (CIs).<sup>6</sup> These energized intermediates rapidly undergo either unimolecular decay to hydroxyl radicals<sup>7</sup> or collisional stabilization.<sup>8</sup> Stabilized CIs can isomerize and decompose into products including the OH radical, or undergo bimolecular reactions with water vapor, SO<sub>2</sub>, NO<sub>2</sub> and acids<sup>9,10</sup>.

The smallest CI is formaldehyde oxide (H<sub>2</sub>COO). Laboratory studies required for a more detailed understanding of the spectroscopy and reaction dynamics<sup>11</sup> became possible following successful in situ generation of H<sub>2</sub>COO using photolysis of CH<sub>2</sub>I<sub>2</sub> in O<sub>2</sub>.<sup>12</sup> Earlier computations proposed that energized H<sub>2</sub>COO can decompose to HCO+OH and H<sub>2</sub>CO+O(<sup>3</sup>P) or isomerize to dioxirane. Access to the HCO+OH channel requires H-transfer to form the linear isomer HCOOH. The dioxirane and H-transfer pathways are shown in Figure 1.

Vibrationally induced reactivity has been found to initiate a sequence of chemical transformations in the next-larger CI, *syn*-CH<sub>3</sub>CHOO. Direct time-domain experimental rates for appearance of OH from unimolecular dissociation of *syn*-CH<sub>3</sub>CHOO under collision free conditions were obtained by vibrationally activating the molecules with energies equivalent to approximately two quanta in the CH-stretch vibration<sup>13,14</sup> which is close to the barrier for formation of H<sub>2</sub>CCHOOH and subsequent OH-elimination. Computationally, the entire reaction pathway from energized *syn*-CH<sub>3</sub>CHOO to OH(X<sup>2</sup>Π) elimination was followed

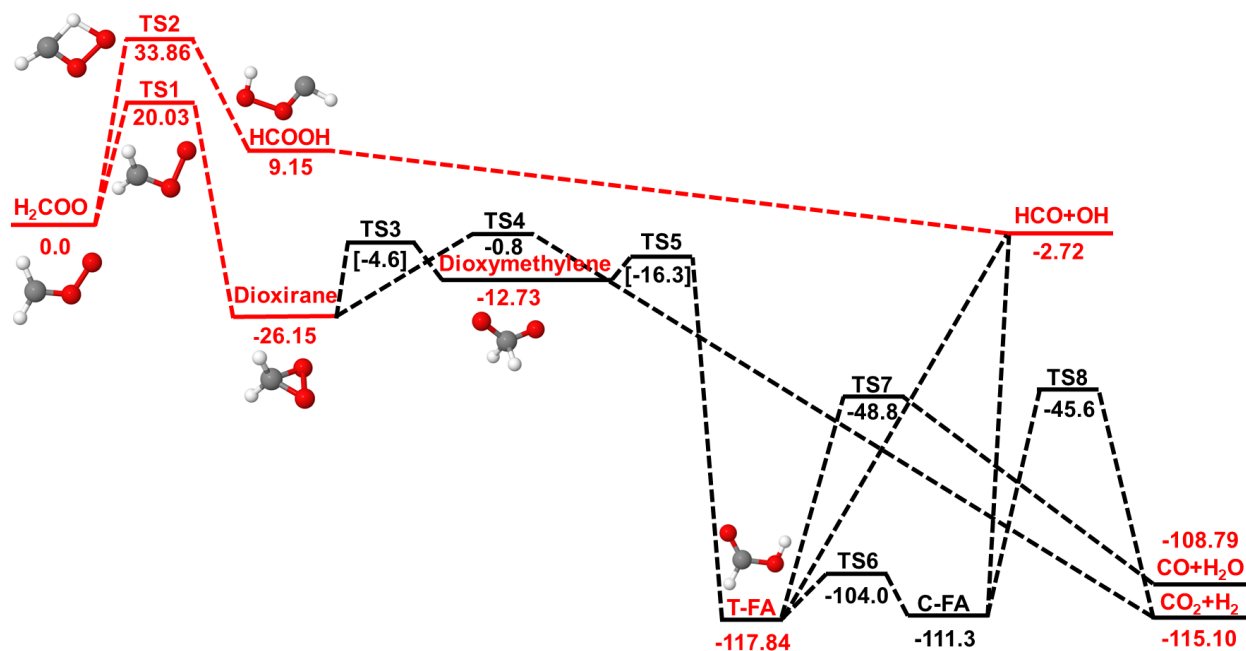


FIG. 1. Decomposition pathways for  $\text{H}_2\text{COO}$  on the singlet PES at the CCSD(T)-F12a/aVTZ level of theory (red). Two reaction channels (red line) are considered in the present work: The H-transfer channel leading to linear  $\text{HCOOH}$  which further decays to  $\text{HCO}+\text{OH}$  and the dioxirane channel which leads to formic acid (FA) and three different final product channels (the H-production channels are omitted for clarity). Here, the reaction channels (black line, energies in black determined at CCSD(T)/aVTZ//B3LYP/aVTZ level, and the energies in the square bracket determined at CCSD(T)/aVTZ//CASSCF(8,8)/cc-pVTZ level) were those from Ref.<sup>17</sup>. The present work investigates the first reactive step along the two pathways. Barriers for formation of the  $\text{CO}+\text{H}_2\text{O}$  and  $\text{CO}_2+\text{H}_2$  are  $\sim 70$  kcal/mol. A third possible pathway involving oxygen-atom insertion into one of the CH-bonds to yield formic acid is not shown in this chart.<sup>17</sup>

using neural network (NN) representations of the potential energy surfaces (PESs).<sup>15</sup> In addition to OH-elimination, OH-roaming and formation of glycolaldehyde was found as an alternative reaction pathway.<sup>16</sup>

Excitation of internal vibrational modes was also proposed as a means for OH-elimination in species relevant to atmosphere chemistry, including  $\text{HONO}$ ,  $\text{HONO}_2$ , or  $\text{HO}_2\text{NO}_2$ . These species can absorb visible radiation and induce vibrational overtone transitions to states with several quanta in the OH stretching vibration.<sup>18</sup> For  $\text{H}_2\text{SO}_4$  (sulfuric acid) vibrationally

induced reactivity by exciting the OH-stretch mode was implicated in photodissociation dynamics forming  $\text{SO}_3$  and water.<sup>19</sup> Subsequent molecular dynamics simulations at various levels of sophistication confirmed that excitation of the OH-stretch with 4 to 5 quanta drives the decomposition of  $\text{H}_2\text{SO}_4$ .<sup>20–22</sup> However, although cavity ring-down spectroscopy successfully probed the asymmetric OH stretching vibration with  $\nu_9 = 4$  and  $\nu_9 = 5$ , vibrationally induced photodissociation dynamics has as yet not been observed directly.<sup>23</sup>

In the present work, the reaction dynamics of the smallest CI,  $\text{H}_2\text{COO}$ , following vibrational excitation of internal vibrational modes is considered in order to characterize two competing, low-energy pathways. Excitation of the CH-stretch mode was demonstrated to initiate chemical processing for *syn*- $\text{CH}_3\text{CHOO}$  both, from experiments<sup>24</sup> and atomistic simulations.<sup>15,16</sup> For  $\text{H}_2\text{COO}$  oxygen-atom elimination requires up to 50 kcal/mol whereas the H-transfer and dioxirane channels feature approximate barrier heights of 34 and 20 kcal/mol, respectively. Following the H-transfer pathway directly yields  $\text{OH}+\text{HCO}$  whereas the dioxirane pathway leads to formic acid which may stabilize through collisions or follow further chemical processing, see Figure 1. First, the methods are presented, followed by a description of the intermolecular interactions and the dynamics and rates of the photodissociation reaction. At the end, conclusions are drawn.

## II. METHODS

In this section the reference electronic structure calculations and the construction of the reactive, multidimensional PESs is described. Two representations are considered in the following: a neural network-based approach using the PhysNet architecture and a more empirical but computationally considerably more efficient multi-state adiabatic reactive MD (MS-ARMD) representation. One important difference between these two representations is that MS-ARMD requires a dedicated model to follow one reaction pathway at a time whereas the NN-based representation is capable of describing the dynamics along both pathways at the same time.



## A. Electronic Structure Calculations

Reference energies were first determined at the explicitly correlated (F12) coupled cluster method with singles, doubles, and perturbative triples<sup>25,26</sup> with the augmented correlation-consistent polarized valence triple- $\zeta$  basis set (CCSD(T)-F12a/aVTZ). For transfer learning, *vide infra*, additional CASPT2/aVTZ calculations were carried out. All electronic structure calculations used the Molpro2019 suite of codes.<sup>27</sup>

Initially,  $\sim 6000$  structures for each  $\text{H}_2\text{COO}$  and Dioxirane were selected from two existing datasets that were used to construct two PIP-NN PESs from reference calculations at the CCSD(T)-F12a/aVTZ level.<sup>28,29</sup> Additional reference structures were generated around the two TSs and all the minima considered in the present work by scanning a regular grid in internal coordinates. Subsequently, the "base model" was trained (see below) using energies and forces at this level of theory. The "base model" was further improved from several rounds of adaptive sampling. This led to a total of 29612 structures covering a wide configurational space covering the H-transfer and dioxirane formation channels.

In order to explore whether alternative feasible reaction channels at the conditions considered in the dynamics simulations exist, one-dimensional rigid scan at the CASPT2 level of theory along the O–O bond for the reactant  $\text{H}_2\text{COO}$  at its minimum energy structure is shown in Figure S2. The potential energy curve along the O–O bond agrees well with existing results at the MRCI-F12 level of theory,<sup>30</sup> where the O–O separation is 1.34 Å at equilibrium, and the well depth is  $\sim 50.0$  kcal/mol. The barriers for O–O dissociation and C–H dissociation with 55.00 and 131.00 kcal/mol are significantly higher than the barriers for H-transfer (35.47 kcal/mol) and dioxirane formation (21.39 kcal/mol). Hence, for exploring the H-transfer and dioxirane channels, there is no need to include reference structures for the  $\text{O} + \text{CH}_2\text{O}$  and  $\text{H} + \text{CHOO}$  channels in the present work. The energy profiles of both reaction channels from different computational levels are shown in Figure S1. Both methods CCSD(T)-F12a and CASPT2 are reliable for developing PESs for the title reaction in this work. Conversely, noticeable underestimation is observed in the results obtained from MRCI(12,11) calculations for the dioxirane formation channel subsequent to the transition state. Hence, MRCI is not the best candidate in this work.

## B. Training of the Neural Network and Transfer Learning

Machine-learned PESs were trained based on the PhysNet architecture,<sup>31</sup> which is designed for predicting energies, forces, dipole moments, and partial charges. The technical background for PhysNet has been detailed in Ref.<sup>31</sup>. By construction, the PhysNet model is permutationally invariant. For the base model, energies, forces and dipole moments for 29612 structures were determined at the CCSD(T)-F12a/aVTZ level of theory. Four independent PhysNet models were trained, using 80% of the data as the training set whereas test and validation sets each contained 10% of the data. The performance on the test data is reported in Figure S3. The best of the four base models was selected for subsequent simulations.

Some of the structural rearrangements are likely to require multi-reference descriptions of the electronic structure. To this end, transfer learning from the CCSD(T)/aVTZ to the CASPT2/aVTZ level of theory was used to improve the PES in regions where multi reference effects may become relevant, for example for O–O bond breaking after H-transfer. Transfer learning (TL) has been shown to be a valuable and resource-efficient technique for developing global potential energy surfaces starting from models based on different initial calculations.<sup>32–36</sup> Here, energies and forces for 2000 structures along the IRCs were used together with several hundred structures around the minima and transition states for both pathways (Figure 1) from which a preliminary TL PES was trained. Next, adaptive sampling was employed to refine the dataset for the TL PES. For this, DMC and short MD simulations with 40.0 kcal/mol excess energy along the CH-stretch mode were run to validate the TL PES and identify deficiencies. The final data set contained 5162 structures for which energies and forces at the CASPT2/aug-cc-pVTZ level were used to train 4 independent models. For TL, the data was split into training (90%), validation (5%), and test set (5%). After that, the best of the four models was chosen for production simulations.

### C. Fitting the MS-ARMD PES

MS-ARMD is a computationally efficient means to investigate chemical reactions based on empirical force fields.<sup>37</sup> The initial parameters for the reactant ( $\text{H}_2\text{COO}$ ) and products ( $\text{HCOOH}$  and dioxirane) were taken from SwissParam<sup>38</sup>. First, the representative structures were sampled from 500 ps MD simulations at 1000 K, and energies were determined at CCSD(T)-F12A/aug-cc-pVTZ level of theory. The force fields for reactant and products were separately parametrized using a downhill simplex algorithm<sup>39</sup>. Several rounds of parameter refinements were done until the root mean squared deviation for the final set between the target (*ab initio*) and the fitted energies for  $\text{H}_2\text{COO}$ ,  $\text{HCOOH}$  and dioxirane reached 0.85/1.5 and 1.07 and 1.7 kcal/mol, respectively. GAPO functions<sup>37</sup> were used to connect reactant and product force fields to yield a continuous, reactive PES along the reaction paths. The transition states for hydrogen transfer and dioxirane formation were 33.83 and 20.33 kcal/mol, respectively, which compare well with reference energies of 33.86 and 20.03 kcal/mol. All parameters for the MS-ARMD PESs are given in the supporting information, see Tables S2 to S5.

### D. Molecular Dynamics Simulations and Analysis

All reactive molecular dynamics simulations were carried out using the CHARMM molecular simulation program<sup>40</sup> including provisions for reactive MD (MS-ARMD) simulations<sup>37,41</sup> and pyCHARMM/PhysNet for the ML/MD simulations.<sup>42,43</sup> All simulations were run in the *NVE* ensemble and in the gas phase. The MD simulations were initiated from the minimized structure of  $\text{H}_2\text{COO}$ , using the PhysNet PESs for pyCHARMM simulations and the MS-ARMD PESs for CHARMM simulations. The time step in all simulations was  $\Delta t = 0.1$  fs to conserve total energy as the bonds involving hydrogen atoms were flexible and each trajectory was run for 1 ns.

For the PhysNet TL PES, simulations involving vibrational excitation were carried out akin to earlier investigations of the photodissociation of syn- $\text{CH}_3\text{CHOO}$ .<sup>15,16</sup> The protocol for obtaining initial coordinates and velocities was as follows. First, the system was heated to

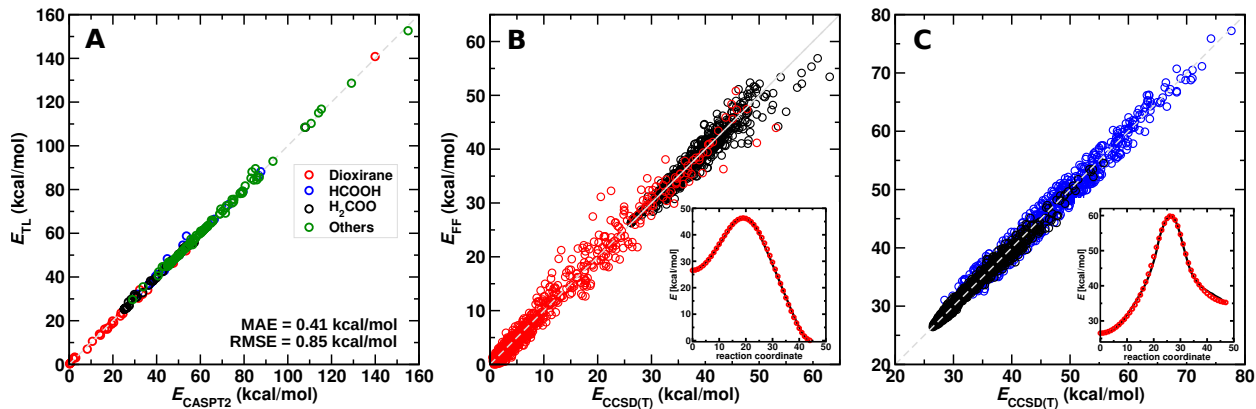


FIG. 2. Correlation of 259 (5%) *ab initio* reference energies and predicted TL energies for the test set from the PhysNet TL model. Panel B: Correlation of the *ab initio* reference structures and the fitted force field for  $\text{H}_2\text{COO}$  (black) and dioxirane (red) with RMSE values of 1.5 and 1.7 kcal/mol respectively. Inset: *ab initio* IRC (red circles) and fitted MS-ARMD (black curve, after GAPOs fitting). Panel C: Correlation of the *ab initio* reference structures and the fitted force field for  $\text{H}_2\text{COO}$  (black) and  $\text{HCOOH}$  (blue) with RMSE values of 0.85 and 1.07 kcal/mol respectively. Inset: *ab initio* IRC (red circles) and fitted MS-ARMD (black curve, after GAPOs fitting).

300 K for 200 ps, followed by equilibration during 50 ps, and a 1 ns production simulation in the microcanonical ( $NVE$ ) ensemble, from which coordinates and velocities were extracted at intervals of 100 fs. This protocol was repeated for 10 independent trajectories. The coordinates and velocities were then utilized as initial conditions for subsequent extensive simulations conducted at various excitation energies.

Following earlier experiments and simulations for  $\text{syn-CH}_3\text{CHOO}$ ,<sup>15,16,44</sup> first excitation along the CH-stretch normal mode was considered. For this, the instantaneous velocity vector was scaled along the normal mode of the CH-stretch vibration such as to yield the desired excitation energy. For the H-transfer channel, excitation energies ranged from 16 to 40 kcal/mol, corresponding to  $\sim 2$  to  $\sim 5$  quanta along the CH-stretch vibration, for which 1000 ( $\sim 2\nu_{\text{CH}}$ ), 1000 ( $\sim 3\nu_{\text{CH}}$ ), 6000 ( $\sim 4\nu_{\text{CH}}$ ) and 3000 ( $\sim 5\nu_{\text{CH}}$ ) independent trajectories were propagated for 1 ns each. The number of quanta considered for the excitation was guided by the barrier heights for the H-transfer and dioxirane channels which are 35.5 and 21.4 kcal/mol, respectively, at the CASPT2/aVTZ level of theory.

Because excitation along the CH-stretch vibration leads to very small numbers of crossings along the dioxirane channel even for the highest excitation energy (46/3000 crossings with 40.0 kcal/mol excitation for a barrier height of 21.4 kcal/mol), different vibrational modes were considered for this pathway. Guided by the minimum dynamic path, discussed further below, excitation along the combination of the CH-stretch and the  $\text{CO}_\text{A}\text{O}_\text{B}$  bending mode ( $\nu_{\text{COO}}$ ) was used. In this case, the instantaneous velocity vector was first scaled such as to excite the CH-stretch vibration with the desired energies which were 16.0 and 24.0 kcal/mol, respectively, corresponding to  $\sim 2\nu_{\text{CH}}$  and  $\sim 3\nu_{\text{CH}}$ . Next, the resulting velocity vector was scaled along the  $\nu_{\text{COO}}$  normal mode to reach total excitation energies of 22.0 and 25.5 kcal/mol, respectively, equivalent to exciting  $\sim (2\nu_{\text{CH}} + 4\nu_{\text{COO}})$  and  $\sim (3\nu_{\text{CH}} + 1\nu_{\text{COO}})$ .

Using MS-ARMD the reactant was heated to 300 K and equilibrated for 50 ps followed by free *NVE* dynamics for 1 ns. Again, coordinates and velocities were saved to obtain 5000 initial conditions for each of the excitation energies. Vibrational excitation was accomplished through the same procedure as for the PhysNet simulations described above. 2000 independent trajectories for each excitation energy were run for 1 ns each.

### III. RESULTS

First, the representations of the PESs are validated with respect to the reference data, followed by a characterization of the reaction dynamics and the rates for formation of HCOOH and dioxirane.

#### A. Validation of the PESs

**PhysNet Base Model:** The performance metrics of the base model on energies and forces for the test set are summarized in Figure S4. The  $\text{MAE}_{\text{train}}(E)$  and  $\text{MAE}_{\text{test}}(E)$  are 0.007, 0.009 kcal/mol, and the corresponding  $\text{RMSE}_{\text{train}}(E)$  and  $\text{RMSE}_{\text{test}}(E)$  are 0.019, 0.062 kcal/mol. For the forces the  $\text{MAE}_{\text{train}}(F)$  and  $\text{MAE}_{\text{test}}(F)$  are 0.022, 0.063 kcal/(mol·Å), and the corresponding  $\text{RMSE}_{\text{train}}(F)$  and  $\text{RMSE}_{\text{test}}(F)$  are 0.251, 0.597

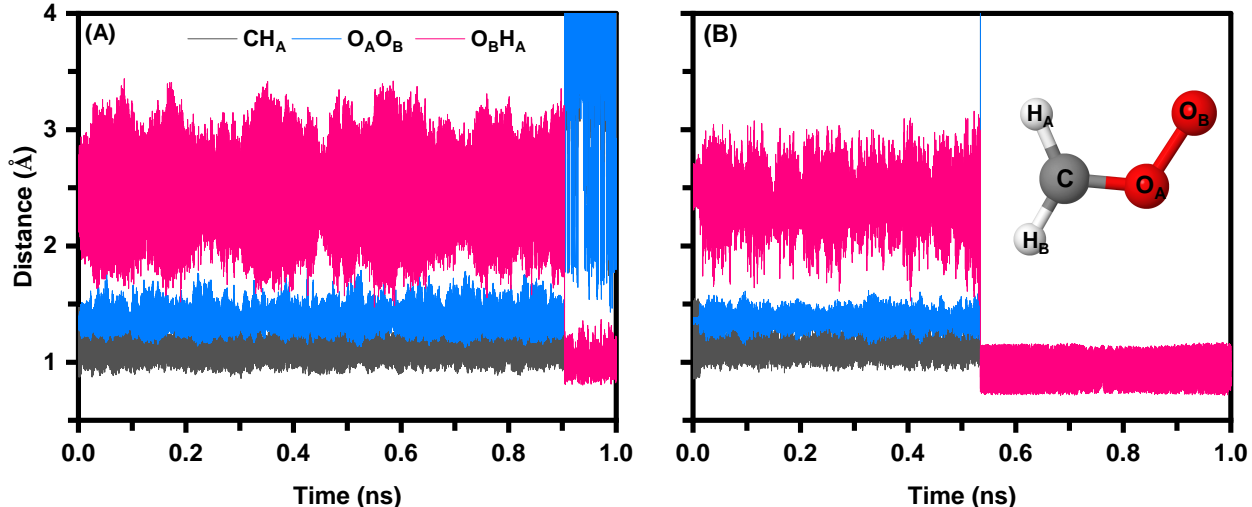


FIG. 3. Time series for  $\text{CH}_A$  (black),  $\text{O}_A\text{O}_B$  (blue), and  $\text{O}_B\text{H}_A$  (pink) separations for a reactive trajectory along the H-transfer channel with  $\sim 4\nu_{\text{CH}}$  (32.0 kcal/mol). Panel A: Using the PhysNet TL PES H-transfer to form linear  $\text{HCOOH}$  occurs at  $t \approx 0.9$  ns (see also Figure S5). Panel B: Using the MS-ARMD PES  $\text{HCOOH}$  forms at  $t \approx 0.5$  ns. The amplitudes for the  $\text{O}_A\text{O}_B$  and  $\text{O}_B\text{H}_A$  separations are comparable whereas for the  $\text{CH}_A$  bond the PhysNet PES is softer.

kcal/(mol·Å), respectively. Optimized structures for the  $\text{H}_2\text{COO}$ , dioxirane,  $\text{HCOOH}$  structures and the TSs connecting them agree to within better than an RMSD of  $10^{-3}$  Å with optimized structures from CCSD(T)-F12 calculations and their energies agree to within better than  $10^{-2}$  kcal/mol, see Table S1. For the harmonic frequencies, the absolute deviations between the predictions for the 5 stationary points and the corresponding *ab initio* values are all smaller than  $6\text{ cm}^{-1}$ , see Figure S6.

For following the reaction it is also of interest to report the minimum energy path and compare the performance of the base model with reference calculations at the CCSD(T)-F12 level, see Figure S7. The RMSD between the reference and PhysNet energies for the test set is 0.063 kcal/mol. Finally, Diffusion Monte Carlo (DMC) simulations were carried out to probe the PES for holes. Propagating 30000 walkers for 50000 steps did not detect a single hole which illustrates the robustness of the PES.

**Transfer Learned Model to CASPT2:** The quality of the PhysNet TL PES is reported in Figure 2. The  $\text{RMSE}(E)$  and  $\text{MAE}(E)$  between reference calculations and inference of

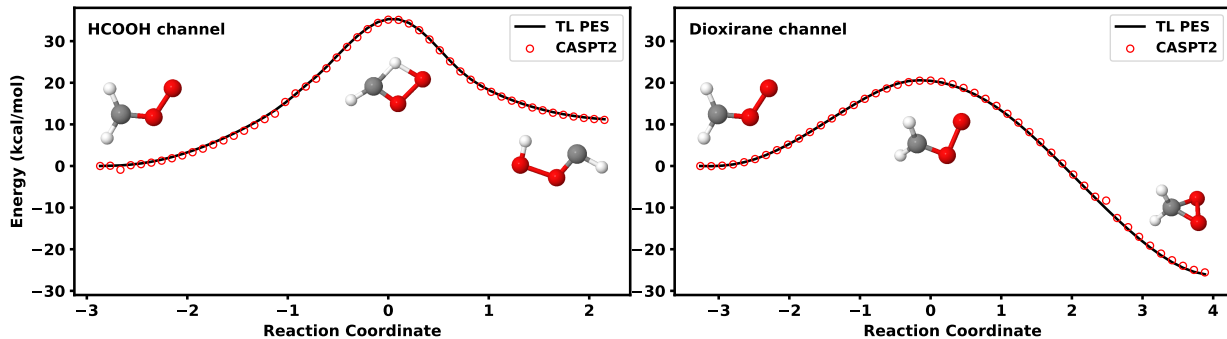


FIG. 4. Energy profiles of the H-transfer channel (left panel) and the dioxirane formation channel (right panel). Here, the black solid line represents the energies from the PhysNet TL model, and the red open circles are the reference (CASPT2) energies.

the NN are 0.85 kcal/mol and 0.41 kcal/mol, respectively. Figure S8 provides additional performance metrics. On energies for the TL model, the  $\text{MAE}_{\text{train}}(E)$  and  $\text{MAE}_{\text{test}}(E)$  are 0.43, 0.41 kcal/mol, and the corresponding  $\text{RMSE}_{\text{train}}(E)$  and  $\text{RMSE}_{\text{test}}(E)$  are 0.91, 0.85 kcal/mol. The  $\text{MAE}_{\text{train}}(F)$  and  $\text{MAE}_{\text{test}}(F)$  on forces for the TL model are 0.39, 0.75 kcal/(mol·Å), and the corresponding  $\text{RMSE}_{\text{train}}(F)$  and  $\text{RMSE}_{\text{test}}(F)$  are 1.46, 3.54 kcal/(mol·Å). Optimized structures at the CASPT2 level and from using the TL-PES agree to within a RMSD of 0.01 Å. Finally, the barrier heights (21.4 and 35.5 kcal/mol for the dioxirane and HCOOH pathways) from CASPT2 calculations and from using the TL-PES differ by 0.81 and 0.22 kcal/mol and the minimum energy paths are reported in Figure 4.

For a more comprehensive evaluation of the TL model’s performance, a limited set of simulations involving the excitation of the CH stretch mode with 32.0 kcal/mol was run. For a single reactive trajectory for the H-transfer channel structures were extracted at regular intervals between reactant and product. Energies for these structures from CASPT/aVTZ calculations (red circles) and from the TL-PES (black line) are compared in Figure 5. With respect to the trained NN-PES all these geometries are off-grid and the agreement between reference and model energies is very encouraging with  $R^2 = 0.96$  and  $\text{RMSE} = 1.58$  kcal/mol, respectively.

**MS-ARMD:** The quality of the MS-ARMD representations of the reactive PESs are reported in Figure 2. The fitted PESs have root mean squared errors of  $\approx 1.0$  kcal/mol

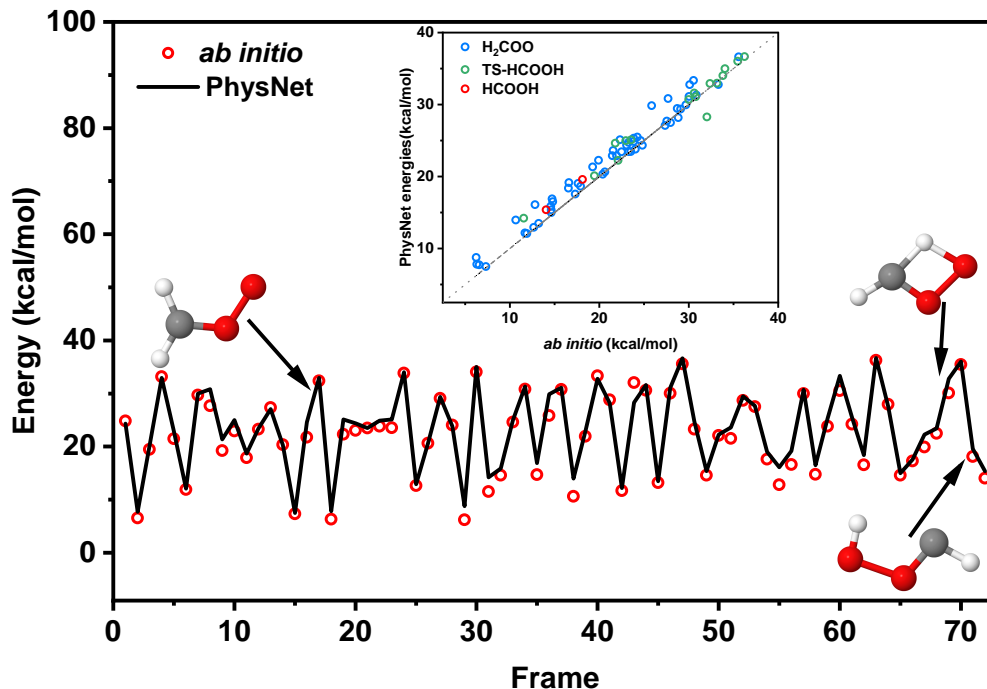


FIG. 5. Main view: Comparison of reference CASPT2 energies (red circles) and predictions from the PhysNet TL model (black line) for a reactive H-transfer trajectory with an excitation energy of 32.0 kcal/mol from reactant to product. The inset shows the corresponding correlation of reference CASPT2 energies and predictions.  $R^2$  and RMSE are 0.96 and 1.58 kcal/mol, respectively.

and the IRC closely follows the reference calculations (see insets). Preliminary simulations were run and energy conservation was observed for both H-transfer and dioxirane channels. Contrary to the machine-learned PESs which allows to simultaneously follow both reaction pathways, MS-ARMD representations can only be used for either H-transfer or dioxirane formation. Hence, no branching ratios can be determined from such simulations.

## B. Reaction Dynamics

For a first impression of the reaction dynamics the minimum dynamic path (MDP) was determined for the two pathways and using the PhysNet TL-PES. Such simulations start from the transition state separating two neighboring minima.<sup>45</sup> The excess energies were  $\Delta E = 0.03$  and 0.11 kcal/mol, respectively, and variations of important internal coordinates along the downhill pathway towards reactant and product for the “H-transfer” and the



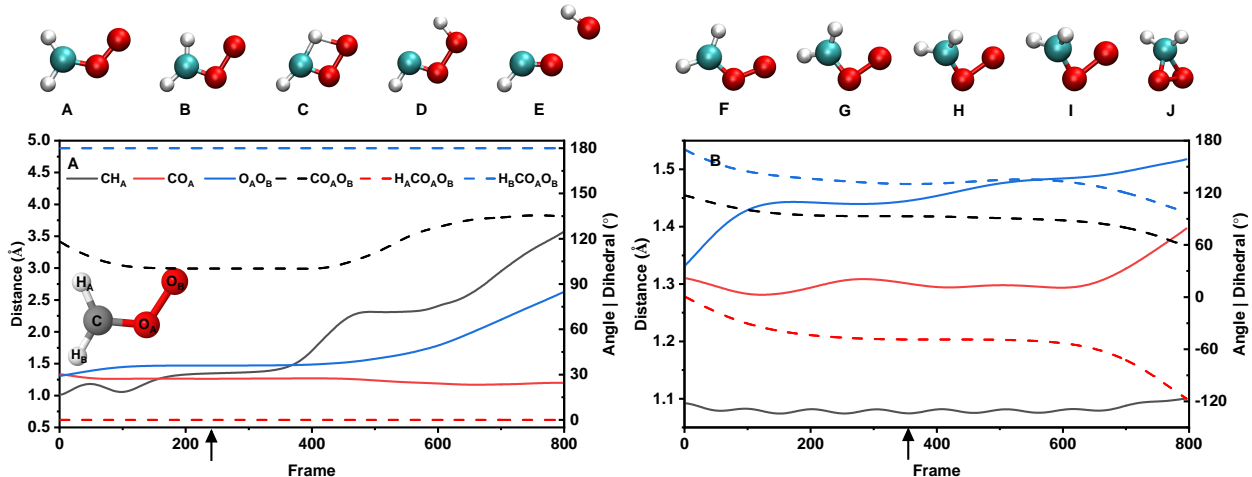


FIG. 6.  $\text{CH}_A$ ,  $\text{CO}_A$  and  $\text{O}_A\text{O}_B$  separations, and change of  $\text{CO}_A\text{O}_B$  angle, and  $\text{H}_A\text{CO}_A\text{O}_B$  and  $\text{H}_B\text{CO}_A\text{O}_B$  dihedrals along the minimum dynamic path from the PhysNet TL PES. Panel A: the H-transfer channel from  $\text{H}_2\text{COO}$  to  $\text{HCOOH}$  and then dissociation to  $\text{OH} + \text{HCO}$ . Panel B: dioxirane formation. Structures A to E and F to J illustrate geometrical arrangements along the pathways. The black arrows indicate the location of the transition states for the H-transfer (frame 234, structure C) and dioxirane (frame 353, structure H) route.

“dioxirane” pathways are reported in Figure 6 for the TL-PES.

For H-transfer the most important participating internal degree of freedom for the reactant  $\rightarrow$  TS step as judged from the MDP is the  $\text{CH}_A$  stretch (solid black). The  $\text{CO}_A$  and  $\text{O}_A\text{O}_B$  separations (solid red and blue) do only change insignificantly in approaching the TS. Similarly, the two dihedral angles (dashed red and blue) do not vary and the chemical transformation occurs in a planar arrangement. There is, however, a readjustment of the  $\text{CO}_A\text{O}_B$  angle (dashed black) from  $118^\circ$  to  $100^\circ$ . These geometrical changes imply that vibrational excitation along the CH-stretch normal mode will be most effective to promote reactivity of  $\text{H}_2\text{COO}$  towards the TS leading to the linear  $\text{HCOOH}$  product and beyond. On the product side it is interesting to note that the  $\text{O}_A\text{O}_B$  distance starts to increase after passing the TS which facilitates breakup towards OH-elimination.

Contrary to that, the dioxirane channel is characterized by an insignificant change along the  $\text{CH}_A$  bond, some variation of the  $\text{CO}_A$  separation, and an increase of the  $\text{O}_A\text{O}_B$  bond

length by 0.1 Å when moving towards the TS. At the same time, all three angles considered decrease in concert. Specifically, the  $\text{CO}_\text{A}\text{O}_\text{B}$  angle changes from  $117^\circ$  to  $92^\circ$ . Taken together, this suggests that sole excitation along the  $\text{CH}_\text{A}$  stretch mode is not expected to be particularly effective for dioxirane formation but a combination band involving the  $\text{CO}_\text{A}\text{O}_\text{B}$  bend may be a good and productive reaction coordinate.

Consequently, two types of vibrational excitations were considered. One used exclusively the  $\text{CH}_\text{A}$  normal mode for which excitation energies of 16 kcal/mol to 40 kcal/mol along this vibration were investigated ( $\sim 2\nu_\text{CH}$  to  $\sim 5\nu_\text{CH}$  quanta). This is akin to previous experimental<sup>44</sup> and computational<sup>15,16</sup> work which also did not employ resonant excitation and the precise number of quanta in a particular degree of freedom is not essential. The second scheme used excitation energies of 22.0 kcal/mol and 25.5 kcal/mol along two CH-stretch/ $\text{COO}$ -bend combinations:  $\sim (3\nu_\text{CH} + \nu_\text{COO})$  and  $\sim (2\nu_\text{CH} + 4\nu_\text{COO})$ .

Figure 7A reports the distribution of  $\text{CO}_\text{A}\text{O}_\text{B}$  angles following excitation with 40.0 kcal/mol ( $\sim 5\nu_\text{CH}$ ) and the ensuing dynamics. Excitation along the CH-normal mode yields almost entirely the linear  $\text{HCOOH}$  isomer. The distribution functions for the reactant (black) and the TS towards linear  $\text{HCOOH}$  (red) clarify that the geometry of the TS towards dioxirane (green dashed line) is virtually never sampled. The maximum of the probability distribution function for the reactant is centered at  $120^\circ$  and extends from  $\sim 90^\circ$  to  $\sim 150^\circ$ . For the transition state towards linear  $\text{HCOOH}$  the maximum shifts to  $100^\circ$  and the distribution narrows considerably, extending only between  $\sim 90^\circ$  and  $\sim 110^\circ$ . The positions of the two maxima are also consistent with the MDP, see Figure 6A. Analysis of these trajectories, (*vide infra*) indicates that all of them develop towards the TS leading to the linear isomer and dioxirane formation is unlikely despite the fact that the excitation energy of  $\sim 40$  kcal/mol is considerably larger than the barrier towards dioxirane (21.4 kcal/mol, see Figure 1). One important reason for this is that the TS leading to dioxirane is characterized by a  $\text{CO}_\text{A}\text{O}_\text{B}$  angle of  $\sim 90^\circ$  (green dashed line in Figure 7) which is unlikely to be sampled for trajectories in which vibrational excitation occurs along the CH-stretch normal mode only. In other words, using the TL-PES energy transfer between the CH-stretching and the  $\text{COO}$ -bending motion is ineffective on the time scale of the present simulations (1 ns).

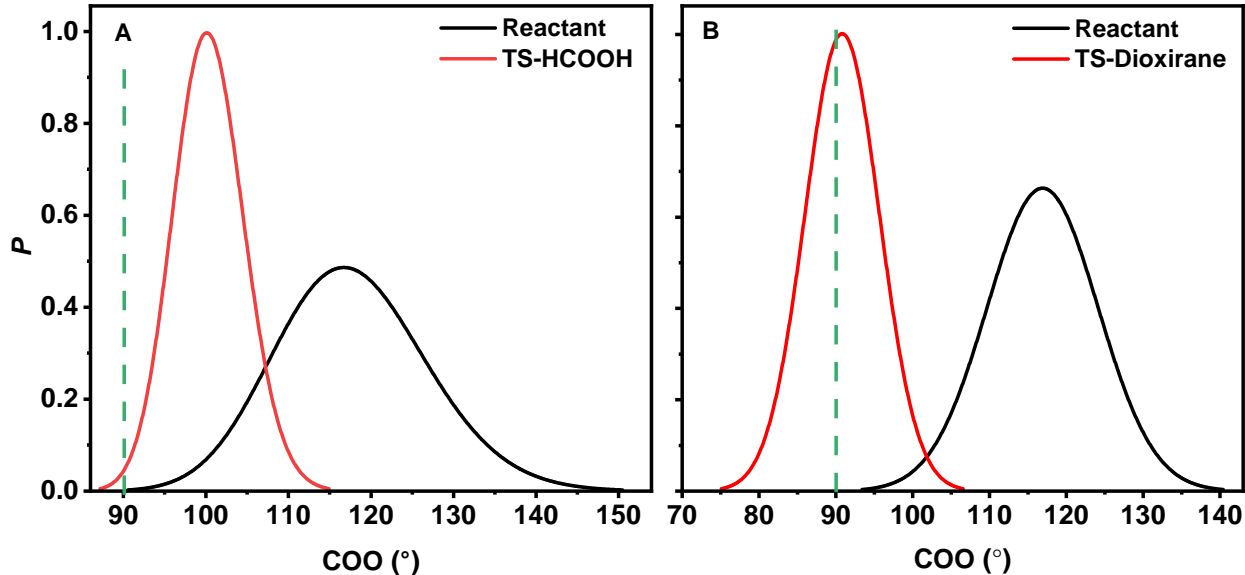


FIG. 7. Panel **A**: Distribution of  $\text{CO}_\text{A}\text{O}_\text{B}$  angle for 2000 reactive trajectories from the simulations with  $\sim 5\nu_{\text{CH}}$  (40.0 kcal/mol) on the PhysNet TL PES for the reactant (black) and the transition state (red) for the linear pathway. The dashed green line indicates the  $\text{CO}_\text{A}\text{O}_\text{B}$  angle at the TS for accessing the dioxirane pathway. As trajectories with excitation exclusively along the  $\text{CH}_\text{A}$  bond do not sample values  $\leq 90^\circ$  for the  $\text{CO}_\text{A}\text{O}_\text{B}$  angle only the linear pathway leading to HCOOH is followed; see text for discussion. Panel **B**: Distribution of  $\text{CO}_\text{A}\text{O}_\text{B}$  angle for 1400 reactive trajectories from the simulations with excitation  $\sim 3\nu_{\text{CH}} + \nu_{\text{COO}}$  (25.5 kcal/mol) on the PhysNet TL PES for the reactant (black) and the transition state (red) for the dioxirane channel. The dashed green line indicates the  $\text{CO}_\text{A}\text{O}_\text{B}$  angle at the TS.

Because the MDP for the linear pathway (see Figure 6A) indicated that the  $\text{CH}_\text{A}$ -stretch changes appreciably and the  $\text{CO}_\text{A}\text{O}_\text{B}$ -bend also varies in approaching the TS, it is of interest to characterize their correlated motion along the reaction pathway. For this, the geometries sampled in the reactant, TS, and product geometries were separately analyzed following excitation with 40.0 kcal/mol, see Figure 8. The black (reactant), red (TS), and blue (HCOOH) point clouds provide a comprehensive description of the motions that are followed for the H-transfer reaction path and clarify that the transition region has finite width, both in the  $\text{CH}_\text{A}$ -stretch and the  $\text{CO}_\text{A}\text{O}_\text{B}$ -bend coordinates, extending well beyond the transition state (yellow cross).

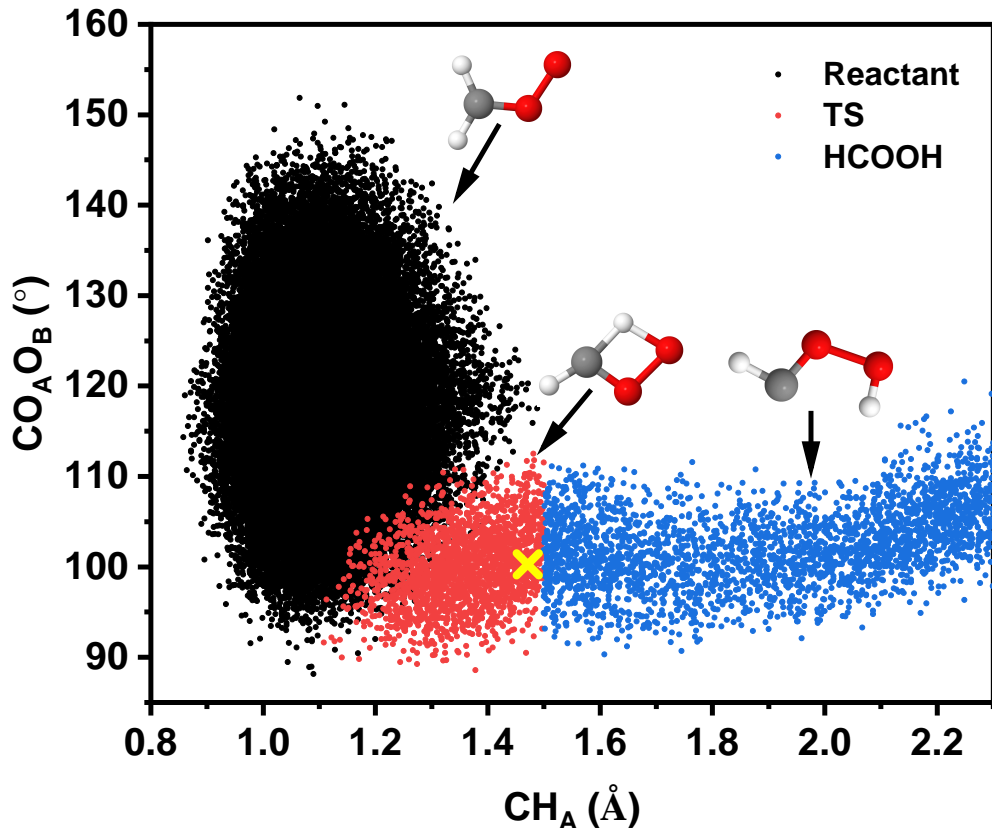


FIG. 8. Correlation between the  $\text{CO}_\text{A}\text{O}_\text{B}$  angle and the  $\text{CH}_\text{A}$  separation for 2500 reactive trajectories from the simulations with 40.0 kcal/mol ( $\sim 5\nu_{\text{CH}}$ ) for the H-transfer channel on the PhysNet TL PES. The width of the transition seam along the  $\text{O}_\text{A}\text{O}_\text{B}$ -separation is 0.4 Å. The yellow cross is at the TS geometry from the CASPT2/aVTZ calculations.

Following excitation of the combination mode with 25.5 kcal/mol, corresponding to  $\sim (3\nu_{\text{CH}} + \nu_{\text{COO}})$ , only the dioxirane pathway is followed. The  $\text{CO}_\text{A}\text{O}_\text{B}$ -distribution functions  $P(\theta_{\text{COO}})$  for the reactant (black) and the TS-geometries (red) leading to dioxirane are reported in Figure 7B together with the  $\text{CO}_\text{A}\text{O}_\text{B}$  angle for the TS from the electronic structure calculations (green dashed line). Evidently, the dynamics samples the TS-geometry extensively and the sampled widths of the distributions decrease in going from the reactant to the TS whereby the TS structure for the linear pathway is only rarely sampled. The correlation between  $\text{O}_\text{A}\text{O}_\text{B}$ -stretch and the  $\text{CO}_\text{A}\text{O}_\text{B}$ -bend coordinates for this pathway is shown in Figure 9. It is interesting to note that product state geometries for the  $\text{O}_\text{A}\text{O}_\text{B}$ -bond lengths are already sampled in the reactant well and the decisive coordinate along the dioxirane-pathway is the  $\text{CO}_\text{A}\text{O}_\text{B}$ -bend.

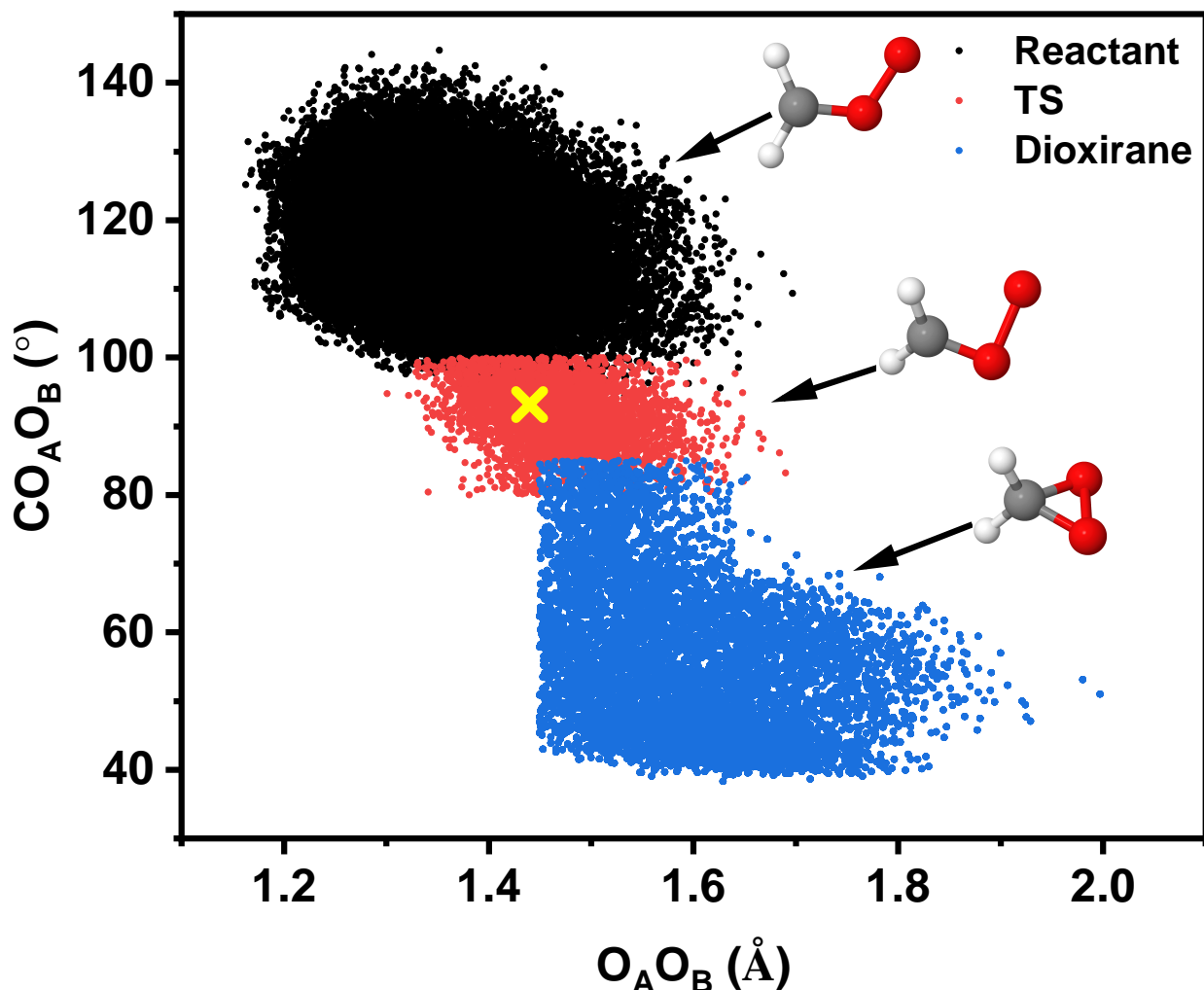


FIG. 9. Distribution of  $\text{CO}_\text{A}\text{O}_\text{B}$  angle as a function of the  $\text{O}_\text{A}\text{O}_\text{B}$  distance for 1400 reactive trajectories from simulations with 25.5 kcal/mol ( $\sim 3\nu_{\text{CH}} + \nu_{\text{COO}}$ ) for the dioxirane channel on the PhysNet TL PES. The width of the transition seam along the  $\text{O}_\text{A}\text{O}_\text{B}$ -separation is 0.4 Å. The yellow cross represents the TS geometry from CASPT2/aVTZ calculations.

### C. Reaction Probabilities

As mentioned earlier, the excitation schemes considered in the present work are chosen to follow the H-transfer or dioxirane-formation pathways. Excitation along the CH-stretch normal mode yields predominantly linear  $\text{HCOOH}$  and only minor amounts of dioxirane even for the highest excitation energy of 40.0 kcal/mol despite a barrier height of only 21.4

kcal/mol to form dioxirane. Conversely, excitation of the CH-stretch/COO-bend combination mode leads exclusively to dioxirane primarily because energies of 22.0 to 25.5 kcal/mol are not sufficient to reach the TS energy towards HCOOH of 33.9 kcal/mol.

TABLE I. Reaction probability for H-transfer channel from simulations by exciting the CH stretch mode with PhysNet TL PES and MS-ARMD force field.

Excitation Energy (kcal/mol)	$\sim 2$ quanta (16.0)	$\sim 3$ quanta (24.0)	$\sim 4$ quanta (32.0)	$\sim 5$ quanta (40.0)
PhysNet ( $E_{\text{TS}}^{\text{CASPT2}} = 35.5$ kcal/mol)	0	0	0.7 %	98.4 %
MS-ARMD ( $E_{\text{TS}}^{\text{CCSD(T)}} = 33.9$ kcal/mol)	0	0	3.0 %	96.0 %

Table I shows that for excitation energies below or close to the barrier height for the H-transfer pathway (33.9 kcal/mol at CCSD(T)/aVTZ and 35.5 kcal/mol at CASPT2/aVTZ) the reaction probability is 0 or a few percent. Excitation with 40.0 kcal/mol ( $\sim 5\nu_{\text{CH}}$ ) leads to formation of HCOOH in almost all cases. Both, the reaction probabilities and the distribution of reaction times agree well for simulations using MS-ARMD and the TL-PES. Because excitation is close to the barrier height with 32.0 kcal/mol ( $\sim 4\nu_{\text{CH}}$ ) the reaction times  $\tau$  are widely distributed, see Figure 10a, and converging them would require a considerably larger number of trajectories. Contrary to that, exciting the CH-stretch normal mode with 40.0 kcal/mol shifts the maximum of the reaction times to short  $\tau$  (Figure 10c).

Following the dioxirane-formation channel features a barrier height of 20.0 and 21.4 kcal/mol at the CCSD(T)/aVTZ and CASPT2/aVTZ levels of theory, respectively, and requires excitation of the CH-stretch/COO-bend combination band. With an excitation energy of 22.0 kcal/mol ( $\sim (2\nu_{\text{CH}} + 4\nu_{\text{COO}})$ ) 96.0 % of the trajectories yield dioxirane if the MS-ARMD PES is used compared with 8.3 % when running the simulations with the TL-PES. Part of this difference arises due to the lower barrier on the MS-ARMD PES. Excitation with 25.5 kcal/mol features 99.0 % compared with 70.3 % of reactive trajectories, see Table II. The reaction time distributions for the two PESs differ quite substantially. Using the MS-ARMD PES,  $P(\tau)$  for excitation with 22.0 kcal/mol peaks at 50.5 ps (blue trace in Figure 10d) compared to 159.2 ps with the TL-PES (red trace in Figure 10d). Excitation with 25.5

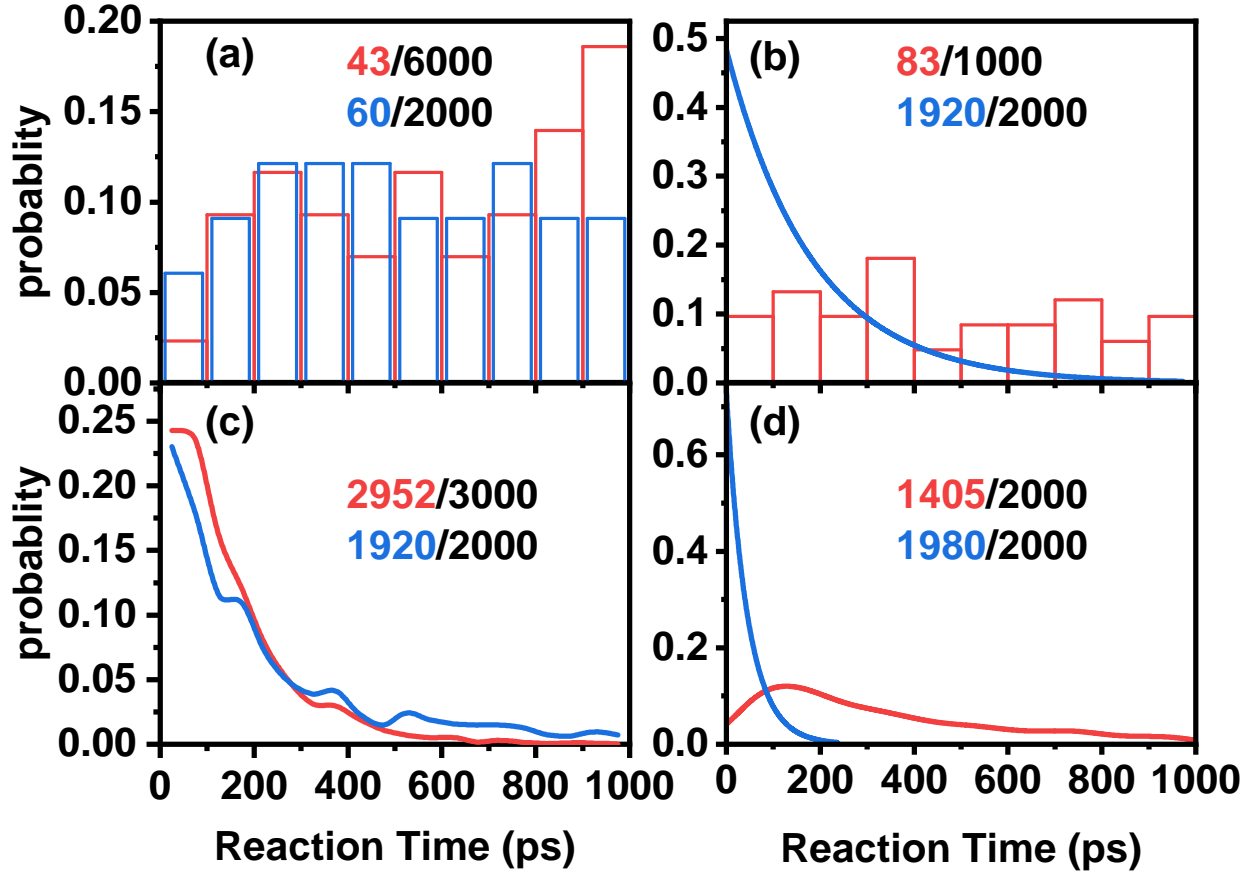


FIG. 10. Normalized reaction time distribution from the MD simulations for the H-transfer (left column) and dioxirane (right column) pathways using the TL-PES (red) and MS-ARMD (blue). Excitation energies in panels a to d are 32.0 kcal/mol ( $\sim 4\nu_{\text{CH}}$ ), 22.0 kcal/mol ( $\sim (2\nu_{\text{CH}} + 4\nu_{\text{COO}})$ ), 40.0 kcal/mol ( $\sim 5\nu_{\text{CH}}$ ), and 25.5 kcal/mol ( $\sim (3\nu_{\text{CH}} + 1\nu_{\text{COO}})$ ), respectively.

kcal/mol broadens all distributions and a multimodal structure for  $P(\tau)$  appears. Again, there is a pronounced peak at early reaction times for simulations using MS-ARMD whereas with TL-PES this feature is missing. Most likely this pronounced peak at short reaction times is due to the lower barrier height of the MS-ARMD PES by 1.4 kcal/mol compared with the TL-PES.

TABLE II. Reaction probability for dioxirane channel from simulations by exciting the CH stretch mode and the COO bending mode with PhysNet base PES, TL PES and MS-ARMD force field.

Excitation Energy (kcal/mol)	$\sim (2\nu_{\text{CH}} + 4\nu_{\text{COO}})$ (22.0)	$\sim (3\nu_{\text{CH}} + 1\nu_{\text{COO}})$ (25.5)
PhysNet ( $E_{\text{TS}}^{\text{CCSD(T)}} = 20.0$ kcal/mol)	20.3 %	67.1 %
PhysNet ( $E_{\text{TS}}^{\text{CASPT2}} = 21.4$ kcal/mol)	8.3 %	70.3 %
MS-ARMD ( $E_{\text{TS}}^{\text{CCSD(T)}} = 20.0$ kcal/mol)	96.0 %	99.0 %

#### IV. DISCUSSION AND CONCLUSION

The present work reports on the reactive dynamics following vibrational excitation of the smallest Criegee intermediate,  $\text{H}_2\text{COO}$ . Excitation of vibrations to drive atmospheric chemical reactions has been used for *syn*- $\text{CH}_3\text{COOH}$ .<sup>15,16,44</sup> and considered for OH-elimination from species such as  $\text{HSO}_3\text{X}$  ( $\text{X} = \text{F}, \text{Cl}, \text{OH}$ ).<sup>23,46</sup> Contrary to these examples, for  $\text{H}_2\text{COO}$  two reaction pathways were considered which lead to different product channels. Importantly, the present work suggests that depending on the vibrational modes that are excited, the two pathways are almost selectively followed from simulations using the TL-PES which allows to access both pathways in the same simulation. If the CH-stretch normal mode is excited with  $\sim 5\nu_{\text{CH}}$  (40.0 kcal/mol), the probability for H-transfer and formation of linear  $\text{HCOOH}$  is two orders of magnitude larger than dioxirane formation. This is despite the fact that the barrier height for formation of dioxirane is only 21.4 kcal/mol at the CASPT/aVTZ level of theory. Conversely, excitation of the COO-bend with energy equivalent to 1 quantum in the  $\nu_{\text{COO}}$  mode is sufficient to yield appreciable amounts of dioxirane using both PESs considered. In other words, mode selective chemistry is observed for  $\text{H}_2\text{COO}$ .

The possibility to deposit energy corresponding to multiple quanta in stretch modes was demonstrated for  $\text{H}_2\text{SO}_4$  for which the  $4\nu_9$  and  $5\nu_9$  O-H stretching overtones were excited.<sup>23</sup> Similarly, vibrational “ladder climbing” was used to deposit up to 4 quanta of vibrational energy in nitrile (-CN) functionalized phenol.<sup>47</sup> Finally, excitation of high vibrational states ( $v \geq 7$ ) of CO-ligands in  $\text{Cr}(\text{CO})_6$  was found to lead to CO-dissociation from the parent molecule.<sup>48</sup> These findings illustrate that excitation of highly excited vibrational states is possible to probe the spectroscopy and even induce reactivity.



Reactive MD simulations were also run using the NN-base model determined from CCSD(T)-F12a/aVTZ reference calculations. Although the quality of the NN-representation is excellent (see e.g. Table S1), excitation along the CH-stretch normal mode often feature problems: for example, C-O bond breaking to form  $\text{CH}_2+\text{O}_2$  is found which should not occur at these excitation energies. In search for a reason it was found that the CCSD(T)-F12a/aVTZ reference data on the singlet PES feature a local minimum for elongations along the C-O stretch coordinate at 1.75 Å, corresponding to an energy of  $\sim 30$  kcal/mol. Although the NN-base model reliably captures this feature, breaking of the CO bond along the singlet-PES at such low energies is not realistic. The reason for this spurious feature is the proximity of the triplet-PES which complicates the electronic structure calculations in this region of configuration space and single-reference methods are not sufficiently reliable.

Using TL based on CASPT2/aVTZ improves the situation in that the spurious minimum is shifted to longer CO-separations and to  $\sim 85$  kcal/mol which is considerably higher than the transition state towards H-transfer at 33.8 kcal/mol. This allows to run meaningful simulations for the processes of interest in the present work. Nevertheless, no globally valid PES is yet available and the CASPT2/aVTZ level of theory does not provide reference data to sufficiently high energies for developing such a PES. For the dioxirane pathway the situation is somewhat better and meaningful simulations for the base model are possible.

From the perspective of atmospheric chemistry, OH-formation from vibrational excitation of  $\text{H}_2\text{COO}$  is most relevant. The present work suggests that excitation of the CH-stretch with  $\sim 4$  to  $\sim 5\nu_{\text{CH}}$  is most likely to yield OH after H-transfer to form linear  $\text{HCOOH}$ . This is comparable to the requirements for decomposition of  $\text{H}_2\text{SO}_4$  through excitation of the OH-stretch.<sup>20,22,49</sup> The pathway through dioxirane involves barriers that are comparable to the stabilization energy of dioxirane itself, hence IVR will limit productive OH-generation, see Figure 1. Finally, the pathway through FA which was not considered here, first involves a very loose transition state (with O-separations of  $\sim 4$  Å from the  $\text{H}_2\text{CO}$ -core at the CASSCF level). Such a TS is very “vulnerable” in an atmospheric environment. Secondly, although the insertion product (c-FA) is highly stabilized by  $-120$  kcal/mol, subsequent barriers are still of the order of 60 to 80 kcal/mol. Thermodynamically, surmounting such

barriers is feasible. However, again, IVR and collisional de-excitation limit this process as has, e.g., been shown for acetaldehyde to form vinoxy-radical.<sup>50</sup>

In summary, the present work explores the reactive dynamics following vibrational excitation of the smallest Criegee intermediate  $\text{H}_2\text{COO}$  at the CCSD(T) and CASPT2 levels of theory. Two different excitation schemes almost exclusively lead to reactive dynamics along the H-transfer and dioxirane-formation pathways. The most promising route for OH-formation involves excitation of the CH-stretch normal mode with energies equivalent to between 4 and 5 quanta to yield  $\text{HCOOH}$  with subsequent breaking of the O–O bond. Although the molecule only contains 5 atoms its electronic structure is challenging and despite the considerable effort in the present and previous work no globally valid, reactive PES is available as of now.

## SUPPORTING INFORMATION AVAILABLE

The PhysNet codes are available at <https://github.com/MMunibas/PhysNet>, and the PhysNet PESs and the data sets containing the reference data can be obtained from <https://github.com/MMunibas/H2COO-PhysNet>.

## ACKNOWLEDGMENT

We thank Prof. Jun Li for providing the datasets for  $\text{H}_2\text{COO}$  and dioxirane. Valuable discussions with Silvan Käser are also acknowledged. This work was supported by China Scholarship Council (to KS), the Swiss National Science Foundation through grants 200020\_219779 and 200021\_215088 and the University of Basel.

## REFERENCES

- <sup>1</sup>D. Stone, L. K. Whalley and D. E. Heard, *Chem. Soc. Rev.*, 2012, **41**, 6348–6404.
- <sup>2</sup>S. Gligorovski, R. Strekowski, S. Barbati and D. Vione, *Chem. Rev.*, 2015, **115**, 13051–13092.
- <sup>3</sup>H. Levy, *Science*, 1971, **173**, 141–143.

- <sup>4</sup>K. Emmerson and N. Carslaw, *Atmos. Environ.*, 2009, **43**, 3220–3226.
- <sup>5</sup>M. Khan, C. Percival, R. Caravan, C. Taatjes and D. Shallcross, *Environ. Sci.: Process. Impacts*, 2018, **20**, 437–453.
- <sup>6</sup>R. Criegee and G. Wenner, *Justus Liebigs Ann. Chem.*, 1949, **564**, 9–15.
- <sup>7</sup>M. S. Alam, M. Camredon, A. R. Rickard, T. Carr, K. P. Wyche, K. E. Hornsby, P. S. Monks and W. J. Bloss, *Phys. Chem. Chem. Phys.*, 2011, **13**, 11002–11015.
- <sup>8</sup>A. Novelli, L. Vereecken, J. Lelieveld and H. Harder, *Phys. Chem. Chem. Phys.*, 2014, **16**, 19941–19951.
- <sup>9</sup>C. A. Taatjes, *Ann. Rev. Phys. Chem.*, 2017, **68**, 183–207.
- <sup>10</sup>R. Mauldin Iii, T. Berndt, M. Sipilä, P. Paasonen, T. Petäjä, S. Kim, T. Kurtén, F. Stratmann, V.-M. Kerminen and M. Kulmala, *Nature*, 2012, **488**, 193–196.
- <sup>11</sup>Y.-P. Lee, *J. Chem. Phys.*, 2015, **143**, 020901.
- <sup>12</sup>O. Welz, J. D. Savee, D. L. Osborn, S. S. Vasu, C. J. Percival, D. E. Shallcross and C. A. Taatjes, *Science*, 2012, **335**, 204–207.
- <sup>13</sup>Y. Fang, F. Liu, V. P. Barber, S. J. Klippenstein, A. B. McCoy and M. I. Lester, *J. Chem. Phys.*, 2016, **144**, 061102.
- <sup>14</sup>Y. Fang, F. Liu, V. P. Barber, S. J. Klippenstein, A. B. McCoy and M. I. Lester, *J. Chem. Phys.*, 2016, **145**, 234308.
- <sup>15</sup>M. Upadhyay and M. Meuwly, *ACS Earth Space Chem.*, 2021, **5**, 3396–3406.
- <sup>16</sup>M. Upadhyay, K. Toöpfer and M. Meuwly, *J. Phys. Chem. Lett.*, **15**, 90–96.
- <sup>17</sup>T.-N. Nguyen, R. Putikam and M.-C. Lin, *J. Chem. Phys.*, 2015, **142**, 124312.
- <sup>18</sup>D. Donaldson, G. Frost, K. Rosenlof and V. Tuck, A.F. Vaida, *Geophys. Res. Lett.*, 1997, **24**, 2651 – 2654.
- <sup>19</sup>V. Vaida, H. G. Kjaergaard, P. E. Hintze and D. J. Donaldson, *Science*, 2003, **299**, 1566–1568.
- <sup>20</sup>Y. Miller and R. B. Gerber, *J. Am. Chem. Soc.*, 2006, **128**, 9594–9595.
- <sup>21</sup>J. Yosa Reyes and M. Meuwly, *J. Phys. Chem. A*, 2011, **115**, 14350–14360.
- <sup>22</sup>J. Yosa Reyes, T. Nagy and M. Meuwly, *Phys. Chem. Chem. Phys.*, 2014, **16**, 18533–18544.
- <sup>23</sup>K. J. Feierabend, D. K. Havey, S. S. Brown and V. Vaida, *Chem. Phys. Lett.*, 2006, **420**, 438 – 442.
- <sup>24</sup>F. Liu, J. M. Beames, A. S. Petit, A. B. McCoy and M. I. Lester, *Science*, 2014, **345**, 1596–1598.

- <sup>25</sup>T. B. Adler, G. Knizia and H.-J. Werner, *J. Chem. Phys.*, 2007, **127**, 221106.
- <sup>26</sup>G. Knizia, T. B. Adler and H.-J. Werner, *J. Chem. Phys.*, 2009, **130**, 054104.
- <sup>27</sup>H.-J. Werner, P. J. Knowles, P. Celani, W. Györffy, A. Hesselmann, D. Kats, G. Knizia, A. Köhn, T. Korona, D. Kreplin, R. Lindh, Q. Ma, F. R. Manby, A. Mitrushenkov, G. Rauhut, M. Schütz, K. R. Shamasundar, T. B. Adler, R. D. Amos, S. J. Bennie, A. Bernhardsson, A. Berning, J. A. Black, P. J. Bygrave, R. Cimiraglia, D. L. Cooper, D. Coughtrie, M. J. O. Deegan, A. J. Dobbyn, K. Doll, M. Dornbach, F. Eckert, S. Erfort, E. Goll, C. Hampel, G. Hetzer, J. G. Hill, M. Hodges, T. Hrenar, G. Jansen, C. Köppl, C. Kollmar, S. J. R. Lee, Y. Liu, A. W. Lloyd, R. A. Mata, A. J. May, B. Mussard, S. J. McNicholas, W. Meyer, T. F. Miller III, M. E. Mura, A. Nicklass, D. P. O’Neill, P. Palmieri, D. Peng, K. A. Peterson, K. Pflüger, R. Pitzer, I. Polyak, M. Reiher, J. O. Richardson, J. B. Robinson, B. Schröder, M. Schwilk, T. Shiozaki, M. Sibaev, H. Stoll, A. J. Stone, R. Tarroni, T. Thorsteinsson, J. Toulouse, M. Wang, M. Welborn and B. Ziegler, *MOLPRO, 2019.1* , a package of *ab initio* programs, see.
- <sup>28</sup>J. Li, S. Carter, J. M. Bowman, R. Dawes, D. Xie and H. Guo, *J. Phys. Chem. Lett.*, 2014, **5**, 2364–2369.
- <sup>29</sup>J. Li and H. Guo, *J. Phys. Chem. A*, 2016, **120**, 2991–2998.
- <sup>30</sup>R. Dawes, B. Jiang and H. Guo, *J. Am. Chem. Soc.*, 2015, **137**, 50–53.
- <sup>31</sup>O. T. Unke and M. Meuwly, *J. Chem. Theory Comput.*, 2019, **15**, 3678–3693.
- <sup>32</sup>S. Käser, J. O. Richardson and M. Meuwly, *J. Chem. Theory Comput.*, 2022, **18**, 6840–6850.
- <sup>33</sup>S. Käser and M. Meuwly, *J. Chem. Phys.*, 2023, **158**, 214301.
- <sup>34</sup>S. Käser, L. I. Vazquez-Salazar, M. Meuwly and K. Töpfer, *Digital Discovery*, 2023, **2**, 28–58.
- <sup>35</sup>S. Käser and M. Meuwly, *Phys. Chem. Chem. Phys.*, 2022, **24**, 5269–5281.
- <sup>36</sup>J. S. Smith, B. T. Nebgen, R. Zubatyuk, N. Lubbers, C. Devereux, K. Barros, S. Tretiak, O. Isayev and A. E. Roitberg, *Nat. Comm.*, 2019, **10**, 2903.
- <sup>37</sup>T. Nagy, J. Yosa Reyes and M. Meuwly, *J. Chem. Theory Comput.*, 2014, **10**, 1366–1375.
- <sup>38</sup>V. Zoete, M. A. Cuendet, A. Grosdidier and O. Michielin, *J. Comput. Chem.*, 2011, **32**, 2359–2368.
- <sup>39</sup>J. A. Nelder and R. Mead, *Comput. J.*, 1965, **7**, 308–313.

- <sup>40</sup>B. R. Brooks, C. L. Brooks, III, A. D. Mackerell, Jr., L. Nilsson, R. J. Petrella, B. Roux, Y. Won, G. Archontis, C. Bartels, S. Boresch, A. Caffisch, L. Caves, Q. Cui, A. R. Dinner, M. Feig, S. Fischer, J. Gao, M. Hodoscek, W. Im, K. Kuczera, T. Lazaridis, J. Ma, V. Ovchinnikov, E. Paci, R. W. Pastor, C. B. Post, J. Z. Pu, M. Schaefer, B. Tidor, R. M. Venable, H. L. Woodcock, X. Wu, W. Yang, D. M. York and M. Karplus, *J. Comput. Chem.*, 2009, **30**, 1545–1614.
- <sup>41</sup>J. Danielsson and M. Meuwly, *J. Chem. Theory Comput.*, 2008, **4**, 1083.
- <sup>42</sup>K. Song, S. Käser, K. Töpfer, L. I. Vazquez-Salazar and M. Meuwly, *J. Chem. Phys.*, 2023, **159**, 024125.
- <sup>43</sup>J. Buckner, X. Liu, A. Chakravorty, Y. Wu, L. F. Cervantes, T. T. Lai and C. L. Brooks III, *J. Chem. Theory Comput.*, 2023, in print.
- <sup>44</sup>N. M. Kidwell, H. Li, X. Wang, J. M. Bowman and M. I. Lester, *Nat. Chem.*, 2016, **8**, 509–514.
- <sup>45</sup>O. T. Unke, S. Brickel and M. Meuwly, *J. Chem. Phys.*, 2019, **150**, 074107.
- <sup>46</sup>S. Brickel and M. Meuwly, *J. Phys. Chem. A*, 2017, **121**, 5079–5087.
- <sup>47</sup>J. P. Kraack and P. Hamm, *Phys. Chem. Chem. Phys.*, 2016, **18**, 16088–16093.
- <sup>48</sup>T. Witte, T. Hornung, L. Windhorn, D. Proch, R. de Vivie-Riedle, M. Motzkus and K.-L. Kompa, *J. Chem. Phys.*, 2003, **118**, 2021–2024.
- <sup>49</sup>D. J. Donaldson, A. F. Tuck and V. Vaida, *Chem Rev*, 2003, **103**, 4717 – 4729.
- <sup>50</sup>S. Käser, O. T. Unke and M. Meuwly, *J. Chem. Phys.*, 2020, **152**, 214304.
- <sup>51</sup>A. Rohatgi, *Webplotdigitizer: Version 4.6*, 2022, <https://automeris.io/WebPlotDigitizer>.
- <sup>52</sup>H.-G. Yu, S. Ndengue, J. Li, R. Dawes and H. Guo, *J. Chem. Phys.*, 2015, **143**, 084311.
- <sup>53</sup>Y.-H. Huang, J. Li, H. Guo and Y.-P. Lee, *J. Chem. Phys.*, 2015, **142**, 214301.

SUPPORTING INFORMATION: OH-Formation Following Vibrationally Induced Reaction Dynamics of H<sub>2</sub>COO

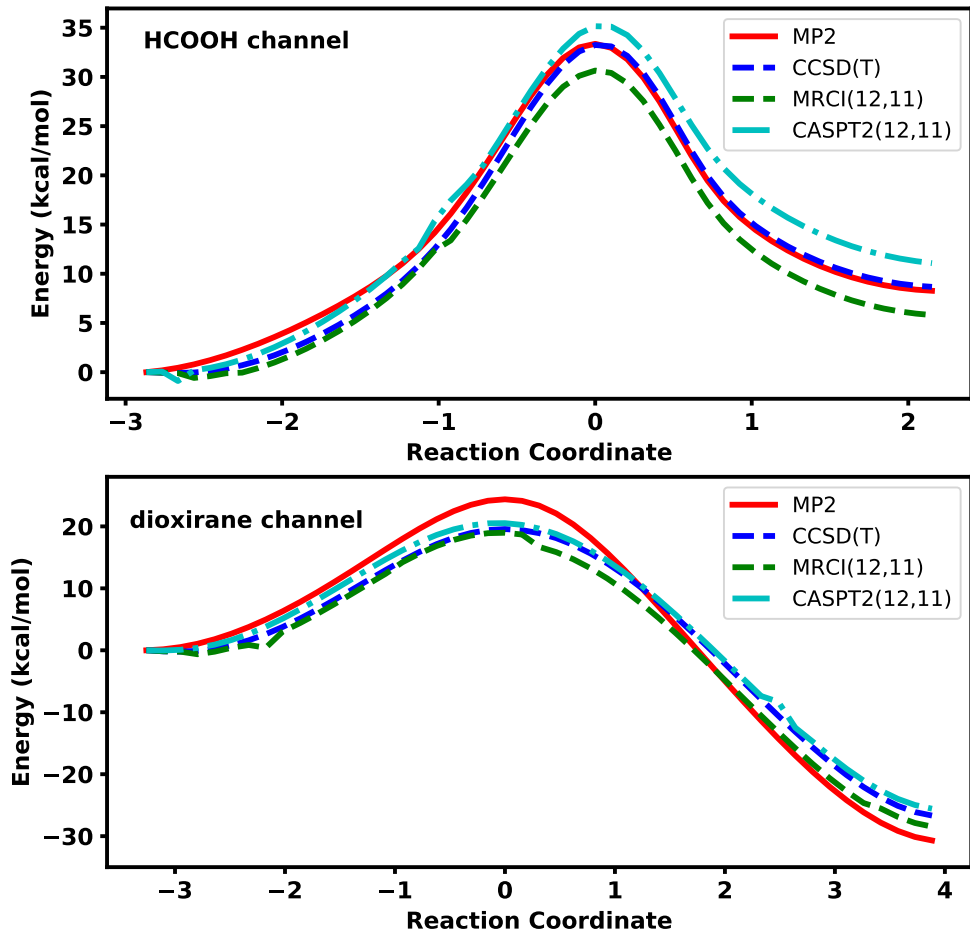


FIG. S1. The energy profiles of H<sub>2</sub>COO for the H-transfer channel (upper panel) and for the dioxirane channel (bottom panel). The performance of three different level of theory (MP2, CCSD(T), MRCI, CASPT2) are included for comparison.

TABLE S1. Comparison of energies for 5 stationary points between the predicted energies and *ab initio* energies (in kcal/mol) from the PhysNet base model.

	H <sub>2</sub> COO	TS-dioxirane	Dioxirane	TS-HCOOH	HCOOH
CCSD(T)	0.00	20.03	-26.15	33.86	9.15
base model	0.00	20.03	-26.15	33.86	9.15

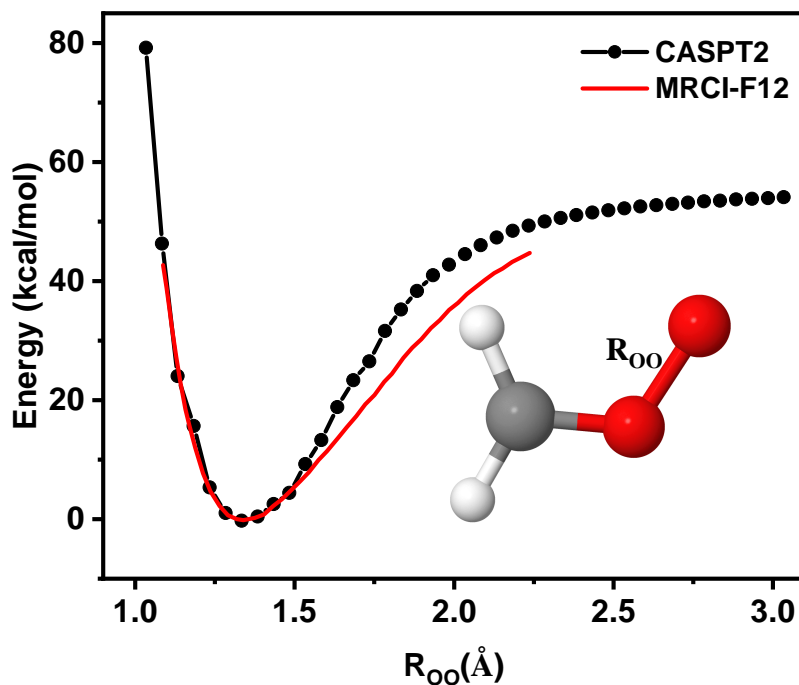


FIG. S2. One-dimensional cut at CASPT2 level of theory for the reactant along the O-O bond with other coordinates fixed at the equilibrium of H<sub>2</sub>COO. The relaxed scan along the O-O bond (red line) at the MRCI-F12 level from Ref.<sup>30</sup> is included for comparison. For this, the data was extracted from Figure 1 of Ref.<sup>30</sup> using WebPlotDigitizer<sup>51</sup> for graphical representation.

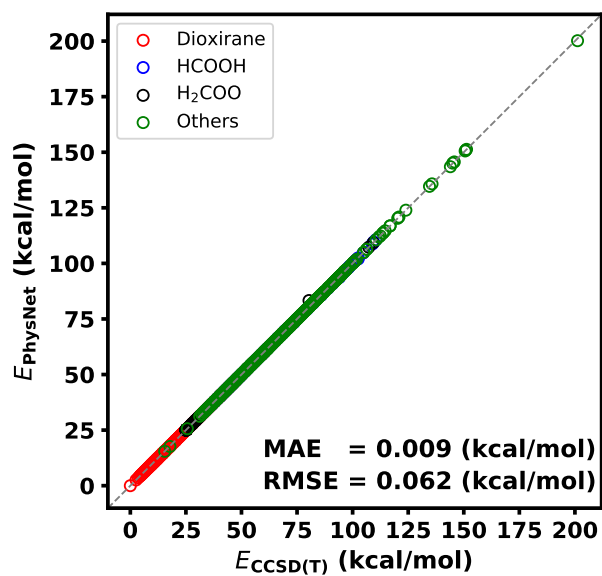


FIG. S3. Correlation of 2962 (10%) *ab initio* energies and predicted energies on the test set from the PhysNet base model.

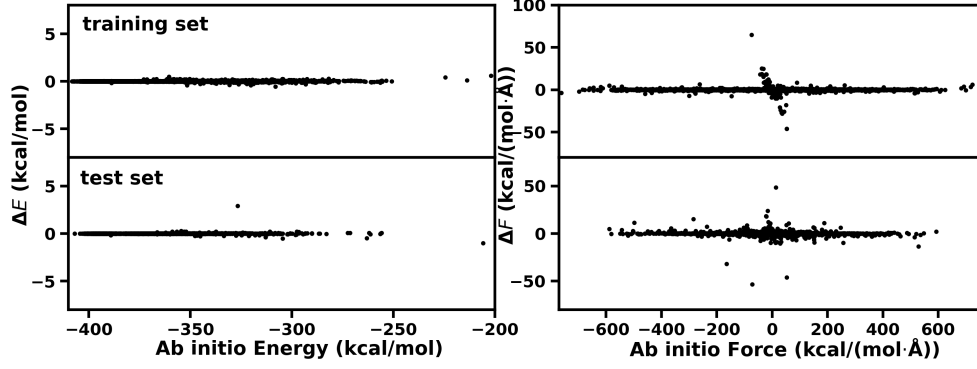


FIG. S4. Comparison between reference CCSD(T)-F12a/aVTZ energies/forces and predicted energies/forces on the training and test sets from the PhysNet base model, from top to bottom. The performance of the best PhysNet base model for  $\text{H}_2\text{OOC}$  is shown. Here,  $\Delta E = E_{\text{PhysNet}} - E_{\text{CCSD}}$ ,  $\Delta F = F_{\text{PhysNet}}^\alpha - F_{\text{CCSD}}^\alpha$  where  $\alpha = (x, y, z)$  are the three Cartesian components of the forces on each atom. On the energies for the base model, the  $\text{MAE}_{\text{train}}(E)$  and  $\text{MAE}_{\text{test}}(E)$  are 0.007, 0.009 kcal/mol, and the corresponding  $\text{RMSE}_{\text{train}}(E)$  and  $\text{RMSE}_{\text{test}}(E)$  are 0.019, 0.062 kcal/mol. The  $\text{MAE}_{\text{train}}(F)$  and  $\text{MAE}_{\text{test}}(F)$  on forces for the model are 0.022, 0.063 kcal/(mol·Å), and the corresponding  $\text{RMSE}_{\text{train}}(F)$  and  $\text{RMSE}_{\text{test}}(F)$  are 0.251, 0.597 kcal/(mol·Å).



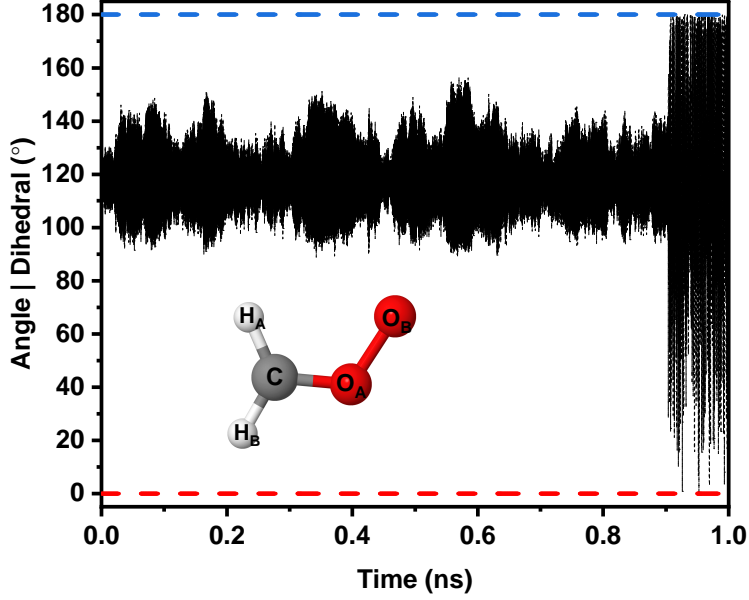


FIG. S5. Time series for  $\text{CO}_\text{A}\text{O}_\text{B}$  valence angle (black) and  $\text{H}_\text{A}\text{CO}_\text{A}\text{O}_\text{B}$  (red) and  $\text{H}_\text{B}\text{CO}_\text{A}\text{O}_\text{B}$  dihedrals (blue) for a reactive trajectory for the H-transfer channel by exciting  $\sim 4\nu_{\text{CH}}$  (32.0 kcal/mol) using the PhysNet TL PES. H-transfer occurs after  $\sim 0.9$  ns. The molecule remains planar throughout the simulation.

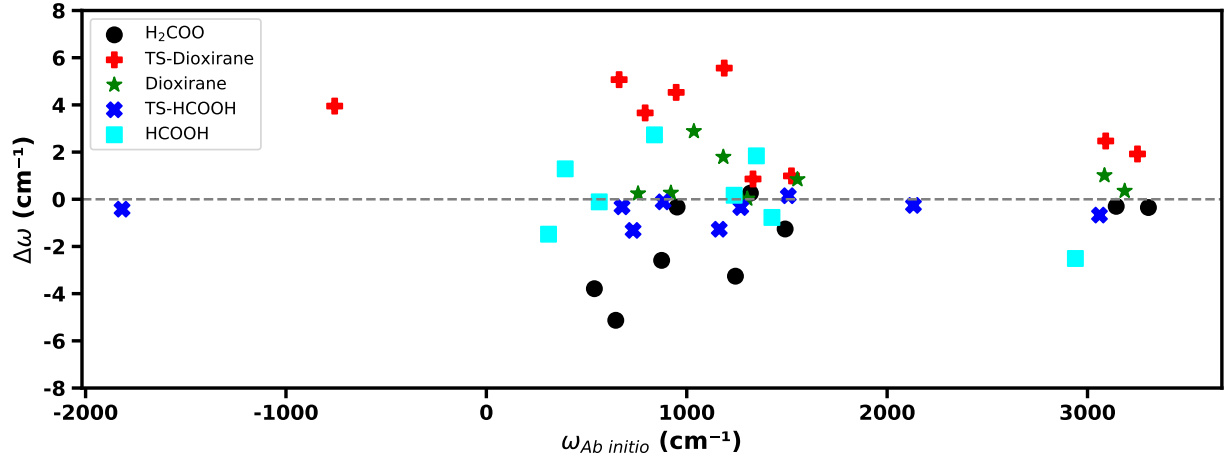


FIG. S6. Accuracy of the harmonic frequencies from the PhysNet base model is shown, with respect to the appropriate reference *ab initio* values. Here,  $\Delta\omega = \omega_{\text{Ab initio}} - \omega_{\text{PhysNet}}$ . All absolute deviations of the harmonic frequencies are smaller than  $6 \text{ cm}^{-1}$ . The measured experimental (anharmonic) frequencies are 847.44, 909.26, 1213.30, 1285.90 and  $1434.10 \text{ cm}^{-1}$ , compared with 872.20, 951.50, 1239.90, 1318.10 and  $1490.0 \text{ cm}^{-1}$  from the base model.<sup>52,53</sup>

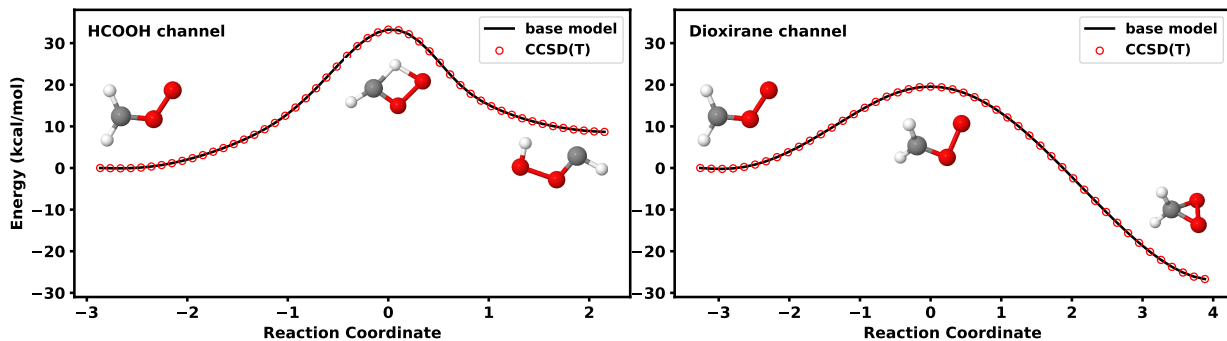


FIG. S7. Energy profiles of the H-transfer channel (left panel) and the dioxirane formation channel (right panel). Here, the black solid line represents the energies from the PhysNet base model, and the red open circles refer to the reference CCSD(T)-F12a/aVTZ energies.

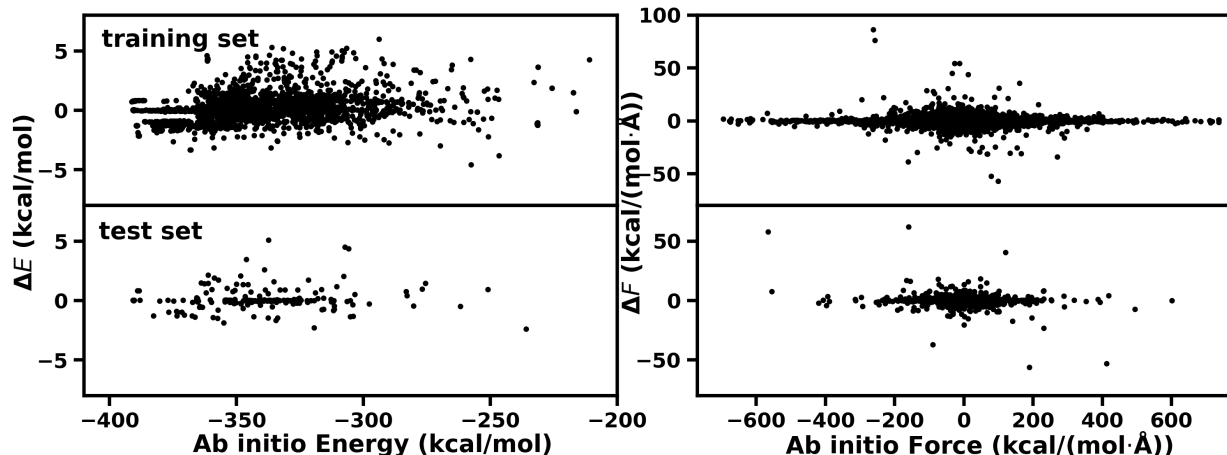


FIG. S8. Comparison between reference CASPT2/aVTZ energies/forces and predicted energies/forces on the training and test sets from the PhysNet TL model, from top to bottom. The performance of the best PhysNet TL model for  $\text{H}_2\text{OOC}$  is shown. Here,  $\Delta E = E_{\text{PhysNet}} - E_{\text{CCSD}}$ ,  $\Delta F = F_{\text{PhysNet}}^\alpha - F_{\text{CCSD}}^\alpha$  where  $\alpha = (x, y, z)$  are the three Cartesian components of the forces on each atom. On the energies for the TL model, the  $\text{MAE}_{\text{train}}(E)$  and  $\text{MAE}_{\text{test}}(E)$  are 0.43, 0.41 kcal/mol, and the corresponding  $\text{RMSE}_{\text{train}}(E)$  and  $\text{RMSE}_{\text{test}}(E)$  are 0.91, 0.85 kcal/mol. The  $\text{MAE}_{\text{train}}(F)$  and  $\text{MAE}_{\text{test}}(F)$  on forces for the model are 0.39, 0.75 kcal/(mol·Å), and the corresponding  $\text{RMSE}_{\text{train}}(F)$  and  $\text{RMSE}_{\text{test}}(F)$  are 1.46, 3.54 kcal/(mol·Å).

Reactant					Product			
Bond harmonic	$k_b$	$r_e$			$k_b$	$r_e$		
1 - 2	410.12	1.08			473.13	1.09		
1 - 3	410.12	1.08			473.13	1.09		
1 - 4	474.32	1.27			437.81	1.38		
4 - 5	203.53	1.34			242.86	1.52		
Bond Morse	$D_e$	$r_e$	$\beta$		$D$	$r_e$	$\beta$	
1 - 5	X	X	X		127.75	1.38	2.69	
Angle	$k_\theta$	$\theta_e$			$k_\theta$	$\theta_e$		
2 - 1 - 3	26.39	121.99			20.13	135.59		
2 - 1 - 4	46.27	116.96			54.50	118.82		
3 - 1 - 4	53.38	113.91			67.83	117.68		
1 - 4 - 5	39.38	121.72			67.78	120.94		
4 - 1 - 5	X	X			22.97	89.04		
2 - 1 - 5	X	X			82.66	106.65		
3 - 1 - 5	X	X			54.73	118.00		
1 - 5 - 4	X	X			40.18	98.21		
Dihedral	N	$k_d$	$\phi_d$		N	$k_d$	$\phi_d$	
2 - 1 - 4 - 5	2	4.02	180.00		X	X	X	
3 - 1 - 4 - 5	2	5.54	180.00		X	X	X	
Improper	N	$k_i$	$\phi_i$		N	$k_i$	$\phi_i$	
1 - 2 - 4 - 3	0	21.33	0.00		0	18.04	0.00	
1 - 5 - 4 - 2	0	X	X		0	15.26	0.00	
GVDW	$r$	$\epsilon$	n	m	$r$	$\epsilon$	n	m
1 - 5	1.76	0.72	6.19	12.82	X	X	X	X

TABLE S2. The harmonic bond, Morse bond, valence angle and generalized van der Waals parameters for reactant(CH<sub>2</sub>OO) and product(dioxirane).  $k_b$  in kcal/mol/Å<sup>2</sup>,  $r_e$  in Å,  $D_e$  in kcal/mol,  $\beta$  in Å<sup>-1</sup>,  $k_\theta$  in kcal/mol/radian<sup>2</sup>,  $\theta_e$  in degree,  $k_d$  in kcal/mol,  $\phi_d$  in degree,  $k_i$  in kcal/mol/radian<sup>2</sup>,  $\phi_i$  in degree,  $r$  in Å and  $\epsilon$  in kcal/mol. Atom number code (see Figure S5): C(1), H<sub>A</sub>(2), H<sub>B</sub>(3), O<sub>A</sub>(4), O<sub>B</sub>(5).

$k$	$V_{ij,k}^0$	$\sigma_{ij,k}$	$a_{ij,k0}$	$a_{ij,k1}$	$a_{ij,k2}$	$a_{ij,k3}$
1	-5.36605	3.91184	-2.86507	-0.43938	-0.20009	0.00187
2	13.43213	1.78751	-0.21920	0.27335		
3	5.14916	3.94423	-2.00850			

TABLE S3. GAPO parameters for dioxirane channel:  $i$  labels the reactant,  $j$  labels the product,  $V_{ij,k}^0$  is the center of the Gaussian function (in kcal/mol),  $\sigma_{ij,k}$  is the width of the Gaussian (in kcal/mol) and  $a_{ij}$  is the polynomial coefficient in kcal/mol.

Reactant					Product			
Bond harmonic	$k_b$	$r_e$			$k_b$	$r_e$		
1 - 3	413.90	1.09			333.44	1.10		
1 - 4	719.68	1.28			388.47	1.23		
Bond Morse	$D$	$r_e$	$\beta$		$D$	$r_e$	$\beta$	
1 - 2	78.55	1.08	2.16		X	X	X	
5 - 2	X	X	X		67.21	0.96	1.98	
4 - 5	349.82	1.34	1.02		9.83	1.53	1.00	
Angle	$k_\theta$	$\theta_e$			$k_\theta$	$\theta_e$		
2 - 1 - 3	18.18	106.37			X	X		
2 - 1 - 4	50.22	115.51			X	X		
3 - 1 - 4	59.82	110.03			31.33	101.58		
1 - 4 - 5	99.54	120.17			92.80	111.12		
2 - 5 - 4	X	X			39.59	91.73		
Dihedral	N	$k_d$	$\phi_d$		N	$k_d$	$\phi_d$	
2 - 1 - 4 - 5	2	5.97	180.00		X	X	X	
3 - 1 - 4 - 5	2	7.37	180.00		X	X	X	
3 - 1 - 4 - 5	3	X	X		3	20.52	0.00	
1 - 4 - 5 - 2	2	X	X		2	7.43	180.00	
Improper	N	$k_i$	$\phi_i$		N	$k_i$	$\phi_i$	
1 - 2 - 4 - 3	0	35.41	0.00		X	X	X	
GVDW	$r$	$\epsilon$	n	m	$r$	$\epsilon$	n	m
5 - 2	3.32	1.3	6.90	13.8	X	X	X	X
1 - 2	X	X	X	X	4.61	1.35	6.95	12.86

TABLE S4. The harmonic bond, Morse bond, angle and generalized van der Waals parameters for reactant(CH<sub>2</sub>OO) and product(HCOOH).  $k_b$  in kcal/mol/Å<sup>2</sup>,  $r_e$  in Å,  $D$  in kcal/mol,  $\beta$  in Å<sup>-1</sup>,  $k_\theta$  in kcal/mol/radian<sup>2</sup>,  $\theta_e$  in degree,  $k_d$  in kcal/mol,  $\phi_d$  in degree,  $k_i$  in kcal/mol/radian<sup>2</sup>,  $\phi_i$  in degree,  $r$  in Å and  $\epsilon$  in kcal/mol. Atom number code(see Figure S5): C(1), H<sub>A</sub>(2), H<sub>B</sub>(3), O<sub>A</sub>(4), O<sub>B</sub>(5).

$k$	$V_{ij,k}^0$	$\sigma_{ij,k}$	$a_{ij,k0}$	$a_{ij,k1}$
1	-9.51488	28.24630	-5.64736	-0.11152
2	-0.48168	6.31526	-5.29915	
3	34.98611	15.02948	2.19718	

TABLE S5. GAPO parameters for H-transfer channel:  $i$  labels the reactant,  $j$  labels the product,  $V_{ij,k}^0$  is the center of the Gaussian function (in kcal/mol),  $\sigma_{ij,k}$  is the width of the Gaussian (in kcal/mol) and  $a_{ij}$  is the polynomial coefficient in kcal/mol.